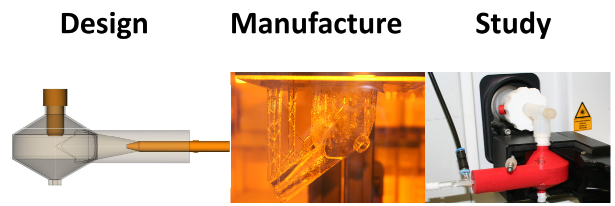

We undertake to print and study cyclone spray chambers by combining and comparing for the first time 3 different printing processes, 5 materials and 8 designs.

3D printing for cyclonic spray chamber in ICP spectrometry

Valérie Geertsen*, Elodie Barruet, Olivier Taché

Commissariat à l'Energie Atomique et aux Energies Alternatives, CEA Saclay, DSM/IRAMIS/NIMBE/LIONS, CNRS UMR 3685, 91191 Gif Sur Yvette, France

valerie.geertsen@cea.fr

Abstract

Additive manufacturing (AM) or 3D-printing is an increasingly widespread technique which is often described as a source for rapid prototyping whereas it is a manufacturing process in itself. It is a new tool for instrumental research laboratories which can now easily manufacture by themselves a large variety of devices. This article describes its application to ICP introduction system spray chambers.

We undertake to print and study cyclone spray chambers by combining and comparing for the first time 3 different AM processes, 5 materials and 8 designs. The analytical performances of these spray chambers are compared with commercial glass and PFA chambers in terms of signal intensity, stability, oxide ratio, LOD and wash-out time.

LOD measured with polymer printed chambers are in the range or even outperform those measured with the glass chamber even though 3D-printed chambers provide lower results in terms of sensitivity than glass. Compared to PFA chamber, the printed chambers are superior in terms of LOD. The printed chambers efficiency is at low temperature AM process and material dependent. SLA and FDM printers give lower results in terms of sensitivity but not in LOD than the Polyjet printer. This study also illustrates side arm nebulizer inner shape influence and confirms the importance a free aerosol recirculation current around the nebulizer tip. Transfer tube efficiency is also questioned, it is found to be weakly detrimental to light elements sensitivity but shows no influence on heavy ones as well as nor on the stability or oxide ratio, whatever the element.

Introduction

In 2012 a normalization organism, The American Society for Testing and Material (ASTM), defined additive manufacturing (AM) as a “process of joining materials to make objects from 3D model data, usually layer upon layer, as opposed to subtractive manufacturing methodologies, such as traditional machining”. Seven AM processes are listed by the ASTM: vat photo-polymerization, material jetting, binder jetting, material extrusion, powder bed fusion, sheet lamination and direct energy deposition. These processes differ from the size of the object they manufacture but also from the material they print and the surface roughness they can achieve. “Additive manufacturing” is a term generally applied to describe the technology overall and more specifically industrial applications and professional high end equipment and applications. Numerous alternative terms to “additive manufacturing” can be found such as “3D printing”, “E-manufacturing”, “freeform fabrication”, …. These terms were coined after “rapid prototyping” which described in a too limited manner the process possibilities and applications. 3D printing is not only a process for rapid prototyping but also a manufacturing technique in itself allowing new designs such as light-weight hollow structures or customized objects. Numerous applications of AM are reported in the literature using commercial printers (e.g. microchip or reaction vessel printing) and with new printing technologies (additive nanomanufacturing for nanolithography, …)[1, 2].

ICP spectrometry is a mature analytical technique which has evolved largely since its appearance in 1980. The technique provides elementary or isotope measurements with good accuracy over a very large concentration range. Its analytical performances (sensitivity, stability, LOD, …) are continuously improving, mainly because of electronic progress. Numerous introduction systems are available[3]. The most common one consists in a pneumatic nebulizer producing a primary aerosol from which coarser droplets are removed in a spray chamber. A tertiary aerosol is then obtained and introduced into the plasma. It is generally accepted that water droplets with diameters smaller than 8 µm should be considered as being the only ones able to complete the sequential process of vaporization, atomization and ionization and contribute to the signal[4]. The aerosol proportion which is analyzed or at least introduced into the plasma is low[5, 6], the maximum attainable analyte transport efficiency for classical spray chambers at high liquid sample flow rate (1mL/min) reaches a few percent. This proportion can be improved both by increasing the number of droplets produced by the nebulizer which are sufficiently small to be analyzed and by optimizing nebulization chamber geometry which must remove coarser droplets but also transport efficiently the smallest ones to the torch.

There are many selection criteria for a specific spray chamber, among them, inner volume, $D_{3,2}$ cutoff diameter, memory effect, signal stability and intensity, oxide ratios, detection limit, equilibration time, transport efficiency, matrix effects, …[7-9] Many chamber geometries have been reported in the literature[10]. Double-pass spray chambers largely used in the past are today mainly replaced by single pass chambers or cyclones. The design of cyclone itself presents numerous variants. Between 1980 and 1982, Greenfield[11], Thelin[12] and Ebdon[13] compared double-pass Scott chambers with 750mL-volume conical cyclones. Cyclone spray chambers were found to transport a greater proportion of aerosol to the plasma than double-pass Scott chambers. The authors reported increases in signal to background ratios by a factor of 1.4 to 2.5. In 1986 A. Montaser et al. reported the study of two 220 and 60mL-cyclone chambers based on the basic configuration of the industrial tall and narrow cyclone[14]. They showed that the signal to background ratios, detection limits and precisions of the analyte signal intensities obtained with the small cyclone chamber were slightly superior to those achieve with a Scott spray chamber or with a gravitational sedimentation chamber[15]. These results were lately confirmed with the study of the commercial so-called Sturman-Master chamber[16-18]. Hieftje and coworkers also proposed vertical cyclones, called rotary cyclones, combining gravitational, centrifugal, turbulent and impact aerosol-sizing mechanisms in a single apparatus[19, 20]. Commercial vortex cyclonic chambers manufactured from various materials (polypropylene, PTFE and glass) were also compared to double-pass Scott chamber[8, 10, 21, 22]. The authors showed that the position of the nebulizer inside the chamber had a noticeable effect on the performances. Cyclones can also include spoilers to deviate the aerosol flow inside the chamber reducing wash-out time[23]. A vertical aerosol transfer tube can be introduced inside the chamber enhancing ICP signal and shortening both wash-out and equilibration times[3].

In spite of the margin of improvement that can be expected from spray chamber optimization, this subject is rarely reported today. This is very probably due the need of glassblowing, an activity which is generally outsourced. Additive manufacturing then appears as a perfect tool to manufacture customized objects in the laboratory itself. Also, the 3D-printing of spray chambers has recently been demonstrated with a low-cost home printer by D.F. Thompson[24].

It is well known that the main phenomena and processes that have to be considered in the spray chamber are aerosol flow turbulence, gas phase compressibility, droplets evaporation, as well as droplets coalescence and impact which are based on gravitational settling or inertial deposition[25]. For vortex cyclone chambers, the impact of droplets on chamber inner surface is the main process involved in the droplets elimination as shown by Schaldach and coworkers. The fluid dynamics phenomena occurring when droplets impact solid or liquid surfaces are very complicated. They depend on many different parameters such as droplet liquid surface tension, viscosity, density and temperature, droplet diameter, impact angle, droplet velocity but also wall physical and chemical properties, surface roughness and temperature[26]. An influence of printing material and fabrication process on spray chamber performances can thus be expected.

We undertake to print and study cyclone spray chambers by combining 3 different AM processes, 5 materials and 8 designs. The analytical performances of these spray chambers are compared with commercial glass and PFA chambers in terms of signal intensity, stability, oxide ratio, LOD and wash-out time. The first part of this work focuses on the influence of the printing process and material, the second one on spray chamber geometry optimization via two distinct studies: the nebulizer side arm and the aerosol transfer tube.

Materials and methods

A 1ppb multi-element solution is prepared by weight dilution in 2% HNO_3 from 1,000 mg/L mono-elemental Li, Co, In, Ce, Ba, Bi, U standards (Spex-CertiPrep, Metuchen, USA). Nitric acid is volume-diluted from Merck 60% ultrapure.

The quadrupole ICPMS is an iCAPQ (ThermoElectron) classically equipped with glass or PFA nebulization chambers cooled by a Peltier device. Glass and PFA commercial chambers are approximately 40mL cyclones and include aerosol transfer tubes. (Figure 1). The comparisons between spray chambers are performed after the instrument automatic tuning which acts on torch position, extraction and focus lenses, and nebulizer gas flow. The entire study is realized with a 1mL/min concentric glass nebulizer (Conikal, Glass Expansion) with natural uptake. The glass spray chamber is regularly tested to confirm the stable day to day performance of the ICPMS. The operating conditions are listed in Table 1.

All measurements (blank and samples) were performed on 6 replicates. Each replicate was a 10-run average measurement. The dwell time was fixed at 0.04s, there were 5 channels per mass, spaced 0.01amu. The LOD was calculated according to the 3 σ criterion, where σ is the standard deviation of 6 blank replicates. The short-term stability (10min) was evaluating calculating the RSD of 40 replicates.

The temperature measurements were realized with a thermocouple directly inserted into the spray chamber transfer tube.

Printed PLA surface modification was realized in a plasma cleaner (Harrick Plasma). The spray chamber was introduced in a reaction enclosure under low vacuum. Low flow rates of oxygen at low pressure were then introduced in the enclosure and submitted to radio frequency electromagnetic radiation creating a plasma at near ambient temperature. The plasma ionized gas molecules interacted with the PLA solid surfaces modifying its physical and chemical characteristics.

Nebulization chamber description

The first set of spray chambers comprises 6 chambers of identical shape (M) but differing materials and / or printing processes. (Table 2). PLA M, PLAD M and PLAcarb M are made with low-cost consumer printers at medium resolution (200µm). PLA M and PLAD M are both printed with high quality polylactic acid filaments (PLA) while PLACarb, a polymer with better layer adhesion then PLA is made of polylactic acid and carbon fiber. PMMA M is printed by jetting through nozzles tiny droplets of liquid or gel-like photopolymer which are instantly UV-cured. This technology provides high-definition printing with 28µm-layers. The polymetacrylate resin chamber (PMA M) is made by medium resolution stereolithography (SLA), an optical system that directs a laser across a tank of liquid resin, solidifying layers as the solid is drawn below the liquid surface. The layers reach 100µm. The PLA O2 is a PLA M chamber treated by cold low-pressure oxygen plasma to increase surface wettability.

The M geometry is illustrated in Figure 2. It is very close to the glass chamber geometry from which it differs by its nebulizer side arm inner shape. The glass spray chamber nebulizer arm is a simple tube attached to the cyclone body. (Figure 1). In the M shape, the nebulizer arm opening is conical for a better evacuation of the very large droplets often stagnating under a high-flow nebulizer.

The second set of chambers is made of 7 PLA cyclones built identically to PLA M but with various side arm dimensions. The chambers are described in Table 3. L is the total arm length and F is the distance over which the nebulizer is fitted inside the arm. (Figure 2). F varies from 11 to 33mm, knowing that the distance between the gas entry and the nebulizer nozzle is 37mm. An example of these chambers is shown on Figure 2. All PLA chambers have conical hollow geometry except PLA R which has a cylindrical geometry.

The printed chambers were designed with FreeCAD, an open source parametric 3D CAD model software (www.freecadweb.org). The freeCAD files created were exported to the printers as *.stl file format. Stl (stereolithography) is a format that only describes the surface geometry of the three-dimensional object. The printer software afterwards slices structures and monitores the manufacturing, each printer having its own slicer software. Whatever the printer used, spray chambers were built horizontally. External pillars were added to support the structure (cyclone bottom and nebulizer side arm) either manually or automatically by the printers' software.

All chambers incorporate central transfer tubes as do the reference Glass and PFA spray chambers. In the case of the 2 commercial chambers, central transfer tubes are attached to the cyclone ceiling, which is impossible for additive building without adding supporting pillars inside the cyclone itself. To circumvent this difficulty, transfer tubes were built separately and inserted into the chambers. This provides opportunity to study the transfer tube geometry effect on the performances. A set of 6 transfer tubes of various lengths were printed in PLA using Replicator 2, one of the filament printer listed in Table 2. An example of a transfer tube I18 is shown on Figure 1. They are noted Ix, x being their total length. The insert used in this study is I22 if not specified otherwise.

Results and discussion

M geometry

Figure 3 compares the entire set of M geometry printed chambers with the glass chamber at ambient temperature. This comparison consists in measuring signal intensities of 4 elements (^{7}Li, ^{59}Co, ^{115}In, ^{238}U) as well as oxide ratios (^{144}Ce^{16}O/^{144}Ce) at various nebulization gas flowrates. The comparison of spray chambers only in terms of signal intensities is reductive as it is easy to enhance signal intensities by increasing nebulizer gas flowrate even if it is detrimental to oxide ratios. On the other hand; fixing nebulization gas flowrate is not judicious as its tuning is poorly reproducible from day to day. Working at fixed oxide ratios is possible but in practice very difficult to realize. Finally, nebulization gas flow value not being an analytical figure of merit in itself we propose more practically to plot the variation of signal intensities versus oxide ratios. Figure 3 has thus been experimentally obtained varying nebulizing gas flowrate between 0.9 and 1.4L/min and measuring signal intensities and oxide ratios. For each gas flowrate, signal intensities are then reported versus oxide ratios. The figure shows a very strong correlation between cerium oxide ratios and signal intensities. It is almost impossible to tune the instrument while keeping the oxide ratios below 2.4% without sacrificing sensitivity. The 5 printed chambers and the glass chamber show close performances despite very different fabrication processes. This result would seem to show that, contrary to what was expected, cyclone chambers which primarily act as impactors are not influenced by their constituent materials.

It is well known that temperature plays a major role for the sensitivity of the introduction system. Vaporizing sample aerosol by convective or infrared heating improves plasma temperature homogeneity and robustness by increasing the analyzable sample amount whereas cooling the spray chamber removes water vapor by condensation, concentrating samples and thus enhancing signal intensities[27]. However it is impossible to heat printed chambers above aerosol vaporization temperature because of the low fusion temperature of filaments or UV-resins. The only alternative is to cool chambers. Figure 4 shows a comparison of the spray chambers at the lowest temperature achievable with the ICPMS cooling device, that is 2°C. Figure S1, providing a view of Figure 4 restricted to oxide ratios from 1.5 to 2.5%, is available in the ESI. The results are very different from those obtained previously. A signal intensity increase is globally observed, confirming the importance of water condensation. It is possible to tune the instrument in order to obtain both oxide ratios below 2.5% and satisfying signal intensities. The polymer printed chambers are even capable of providing satisfying signals until oxide ratio values as low as 1.7% which is impossible for the glass chamber.

It can also be noted that the signal improvement is now material dependent. Glass shows the highest improvement, followed by the PMMA resin whereas the PMA resin and the three PLA exhibit similar improvements. The similarity of the 3 PLA chamber performances indicates the absence of printer or filament influence. Two hypotheses are explored to explain the materials' different behavior towards temperature: the cooling could be more efficient inside the glass chamber compared to the plastic chambers enhancing water condensation or it could be a difference of materials hydrophilic properties.

The first assumption is based on glass and printing materials' thermal conductivity difference. Glass thermal conductivity is of the order 1 W/(m.K) whereas polymers like PMMA or PLA native thermal conductivity is in the range of 0.2-0.4 W/(m.K). It could actually be even less due to the slight porosity introduced by the manufacturing process. A thermocouple is introduced inside the spray chamber transfer tubes at fixed height to measure temperature versus Peltier cooling setting value. These measures show that the best temperature transfer is obtained on the PMMA chamber and not on the glass one. For a 4°C goal temperature, the spray temperature is 8.4°C in the PMMA chamber against 9.5°C for glass and 8.9°C for PLA. This can be easily explained by the slight size difference between the printed chambers and the glass. The printed chambers fit perfectly the Peltier device for an optimized contact whereas the glass chamber being slightly smaller does not touch it on its entire external surface. These measures invalidate the temperature hypothesis as a source of signal variation. It is worth noting that the PLAcarb filament does not transfer heat better than the other PLA despite the presence of 15% of carbon fiber. This is probably due to a circumferential alignment of the fiber that results from the printing process.

The second hypothesis is based on material wettability. An aqueous film is observed on the internal surface of the glass chamber when the droplets emitted by the nebulizer impacts the surface or when the droplets condense on the cooled walls whereas printed chamber inner surfaces cover with drops that magnify until they reach several millimeters and slide down from the wall. To confirm this hypothesis a second PLA M spray chamber is printed and introduced for a few minutes inside a low-pressure cold oxygen plasma enclosure. Cold plasma treatments are classically employed to temporarily modify surface properties increasing wettability or adhesion adding highly reactive functions such as OH groups[28-30]. The surface treatment realized here is very probably of low efficiency as it is difficult in our configuration to create an efficient treatment inside the cyclone. To do so, the plasma must penetrate the cyclone through small openings (drain and transfer tube openings). It is very likely that the oxygen plasma had few contacts with the inner walls. The oxygen plasma treated spray chamber is noted PLA M O2. (Figure 4). The comparison between PLA M and PLAO2 M shows a signal improvement of the four elements studied. It reaches for example 100,000cps for ^{115}In. This improvement is attributed to the surface modification which can be visualized here as a decrease of droplet volume attached to the inner surface chamber. It has to be noted that the importance of water affinity properties for printed material and glass has been pointed out previously but the author proposed to increase polymer hydrophobicity[24]. We promote here on the contrary to increase hydrophilic proprieties.

Another analytical figure of merit in comparing introduction system is the signal stability. Whatever the printed spray chamber tested, the short-term stability evaluated by calculating the RSD from 40 replicates is better than 2%. These results compare very well with the glass chamber showing that, in the conditions tested, the material has no influence on the signal stability.

The wash-out time is also a feature that must be taken into account for evaluating spray chambers. It is calculated here as the time necessary to decrease the signal to 1% of its initial intensity. The results obtained show no material influence. An average value of 17s is necessary to complete wash out whatever the spray chamber.

The LOD is measured on 4 spray chambers at low temperature (glass, PFA, PLA M, PMMA M and PMA M). (Figure 5). The printed chambers generally compare very well and sometimes even outperform the glass chamber. Among the printed chambers, the PMA M shows the best performances with better results than the glass chamber for all elements except barium. The poor results obtained for barium for all printed chambers can be explained by its probable presence at trace levels in the materials themselves. It is also interesting to note the low performances of the PFA chamber. It can be attributed to the PFA chamber blank low stability. PFA blank stability ranges between 5 to 50% for the elements analyzed, when the other chambers' blank stabilities rarely exceed 5%.

This first set of chambers was realized on 4 printers, 3 low-cost home printers (Replicator 2, Ultimaker 2, Form1+) and a professional one (Object30) in order to study the influence of printing quality and more specifically of surface roughness and construction material. An extrusion process as employed in FDM printers leads to ridged surfaces which are detrimental to liquid draining. Imperfections (unfused filament fragments) are also observed, especially on the internal upper surface. Material jetting and vat photo-polymerization produce smoother surfaces without being as smooth as glass or PFA. It is difficult to state on which is the best printing solution (process and material) as each has specific strengths and weaknesses. However this study shows that 3D-printed chambers that can be produced in the laboratory in a few hours for less than 1€ of material even on low-cost printing devices, produce better results in terms of sensitivity and LOD than costly commercial PFA ones. Looking more closely, it appears that the two FDM printers exhibit similar results whatever the analytical figure of merit studied. There is no influence here of filament or printer. The SLA printed chamber PMA M shows poor results in terms of signal intensity but obtains the best results in terms of LOD. If we compare high definition professional and low-cost printers, it appears that the 3 low cost printers give lower results in terms of sensitivity but not in LOD than the high definition professional printer. It is, at this point of the study, impossible to interpret this observation in terms of printing as the limiting factor here is the polymer wettability. Polymer hydrophilic properties must be improved before it is possible to state on the influence of porosity or surface roughness.

Nebulizer arm dimension

The position of the nebulizer tip relative to the nebulization chamber and more precisely to the inner wall of the chamber has proved to be a parameter of great influence on signal intensty[21, 31]. This figure of merit is classically evaluated moving the nebulizer along the cyclone side arm. Additive manufacturing allows here printing several chambers. It is then possible to study the effect on the signal of not only the total arm length L but also of the tip's immediate surroundings. The comparison between PLA M and PLA J illustrates this last point, that is the chamber shape close to the nebulizer tip. (Figure 2). When F is small, the nebulizer is held on a short distance, the tip is unobstructed allowing free circulation of gas flow streamlines. It also diminishes the deposited droplets evacuation slope allowing the formation of larger stagnating droplets under the tip. On the contrary a large F enhances droplets draining, an important feature for chambers made of hydrophobic material. Figure 6 reports the influence of the cyclone side arm geometry on both ^{115}In signal intensity and ^{140}Ce oxide ratio. H and K geometries appear as very detrimental to the signal intensity. They coincide with the two extreme values of L that is 51mm and 91mm giving distances S from the nebulizer tip to the impact surface of 37 for PLA H and 75mm for PLA K. At 37mm from the nebulizer tip, the proportion of droplets in their ballistic phase is probably too high, leading to higher aerosol deposit on the impact area[25, 32]. Conversely, a too long distance to the impact area entails an important reduction of droplet speed decreasing chamber performances. PLA K can be compared with PLA I and PLAJ, the three chambers having the same F distance, that is 31mm and varying arm lengths. I and J geometries show the same performances whereas as described above, the K geometry is clearly unfavorable.

This result is in agreement with a previous study published by Todoli et al in 2000 where the nebulizer position influence is studied for several cyclonic chambers[21]. The authors show that, for a Cinnabar cyclone using an o-ring seal adaptor fastening the nebulizer on a long distance, signal intensity is independent of nebulizer position in a range of at least 7mm. The effect of F at fixed arm length L is illustrated by the comparison of M, L and I geometries. It can be seen that that an optimal geometry is obtained at medium F, that is 21 mm. This is in accordance with Sharp’s observation who recommends placing the nebulizer in the chamber so that the aerosol recirculation current comes from behind the nebulizer tip[32, 33].

It has to be noted that glass and PFA reference chambers geometries are slightly different from those of printed chambers. Glass and PFA chambers have large F distances and flat surfaces under nebulizer tips even if this cylindrical hollow geometry is not efficient in terms of draining. PLA R, a new PLA chamber is manufactured to study the inner shape influence. (Figure 2). PLA R is a PLA cyclone with a side arm cylindrical inner shape. It features the same F and L distances as PLA M and the same F distance as both glass and PFA chambers. Figure 6 shows that PLA R exhibits better sensitivity than PLAM and the best sensitivity of all printed chambers. It illustrates the improvement obtained replacing a conical hollow by a cylindrical one. It shows that inner shape plays an important role in the aerosol distribution inside the cyclone and confirms the importance a free aerosol recirculation current around the nebulizer tip. This subject should be studied precisely in the future to better understand the phenomenon and determine the optimal shape.

Transfer tube

Transfer tubes are often used in cyclonic chamber as a secondary particle separator to help removing larger aerosol particles. They are supposed to reduce solvent load in the plasma without compromising detection limits. Also, they are present in both glass and PFA commercial cyclones. To our knowledge the literature has never reported any study of their real impact. This can be easily explained by the difficulty and cost of performing such a study with glassware. On the contrary this is very easy to realize with 3D-printing. The length of the printed transfer tube varies here from 14mm to 36mm. I26 is a transfer tube with an extremity in the nebulizer horizontal plane, I18 is entirely located in the upper part of the cyclone and I34 reaches the cyclone conical lower part. (Figure 2). Transfer tubes are studied in terms of sensitivity and oxide ratio as described above. The results obtained for the 6 transfer tubes show decreasing impact with element atomic weight. More precisely it shows small influence on light elements sensitivity and no influence on heavy elements as well as no influence on stability or oxide ratio whatever the element. Figure 7 illustrates the results obtained with PMMA M chamber for the lightest element that is ^{7}Li. I14 and I18 which are the shortest transfer tubes tested are the best in terms of sensitivity. These observations can be interpreted as a lack of transfer tube influence on heavy elements and a weak detrimental effect on light elements. This effect is especially disadvantageous as the tube transfer length in the cyclone increases and disturbs the aerosol circulation.

Conclusion

As demonstrated here, 3D printing is much more than a prototyping process, it is a new tool for scientists. The rapid turnaround of the process, the flexibility of design and the low cost of manufacturing provides scientists with previously non-existent possibilities for exploring geometries and materials.

This work demonstrates the applicability of AM for ICP spray chambers and is a basis for future studies. Multiple geometry adjustments of the chamber inner shape have been realized. They illustrate both the influence of the distance between nebulizer tip and the impact area and the importance of aerosol circulation around the nebulizer nozzle. This last specific feature will be more largely developed in the future. These modifications will probably affect outer chamber shape and may require chamber jacket cooling needing more advanced design and manufacturing.

Beyond the modification of shape, 3D-printing with its wide range of printing materials provides a tool for studying the impact on chamber efficiency of other important parameters like the inner wall physical and chemical properties. The PLA polymer oxygen plasma treatment described here is a first example of the impact of the material wettability on signal intensity. 3D printing should contribute to an extensive study of surface treatment to improve sample washing, to reduce further LOD or to provide solutions to classical issues like boron memory effects. This may result in a variety of chambers with tailored surfaces for specific analytes completing existing commodity glass chambers.

Acknowledgment

The authors gratefully acknowledge respectively Thomas Berthelot (CEA), Romain Di Vozzo (Digiteo FabLab) and Kevin Cedrone (FormLabs) for respectively the PMMA M, PLAD M and PMA M chamber printings. The authors also acknowledge the DIM Analytics of the Region Ile de France and the Plateau de Saclay RTRA program for the IcapQ funding.

Parameter	Value
Generator Forward power	1550W
Nebulizer gas flow range	0.8-1.2L/min
Plasma gas flow rate	14L/min
Auxiliary gas flow rate	0.8L/min
Sample flow rate	Natural uptake

Table 1: iCAP Q ICPMS Operating conditions

Chamber	Process	Printer Technology	Printer (Supplier)	Material (Supplier)
PLA M	Material extrusion	FDM	Replicator2 (Makerbot)	PLA (makerbot)
PLAD M	Material extrusion	FDM	Ultimaker2 (Ultimaker)	PLA (ColorFab)
PMA M	Vat photo polymerization	SLA	Form1+ (FormLabs)	PMA resin (FormLabs)
PLAcarb M	Material extrusion	FDM	Replicator2	PLA carbon reinforced (Proto Pasta)
PMMA M	Material jetting	Polyjet	Object30 (Statrasys)	PMMA resin (Statrasys)
PLAO2 M	Material extrusion	FDM	Replicator2	PLA (Makerbot)

Table 2 : Printed chambers with M geometry.

Chamber	L (mm)	F (mm)
PLA H	51	11
PLA G	61	21
PLA I	71	31
PLA L	71	21
PLA M	71	11
PLA J	81	31
PLA K	91	31
PLA R	71	11
Glass	71	20
PFA	71	33

Table 3 : PLA chambers nebulizer side arm geometry.

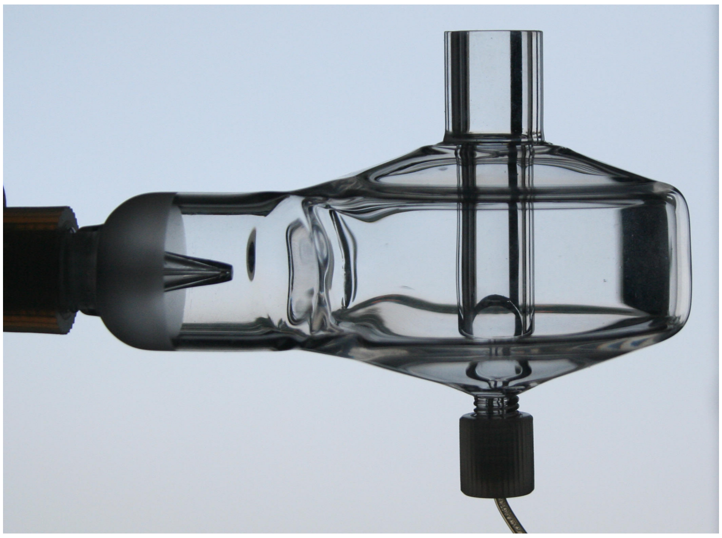

Figure 1 : Side view of the glass spray chamber equipped with the nebulizer

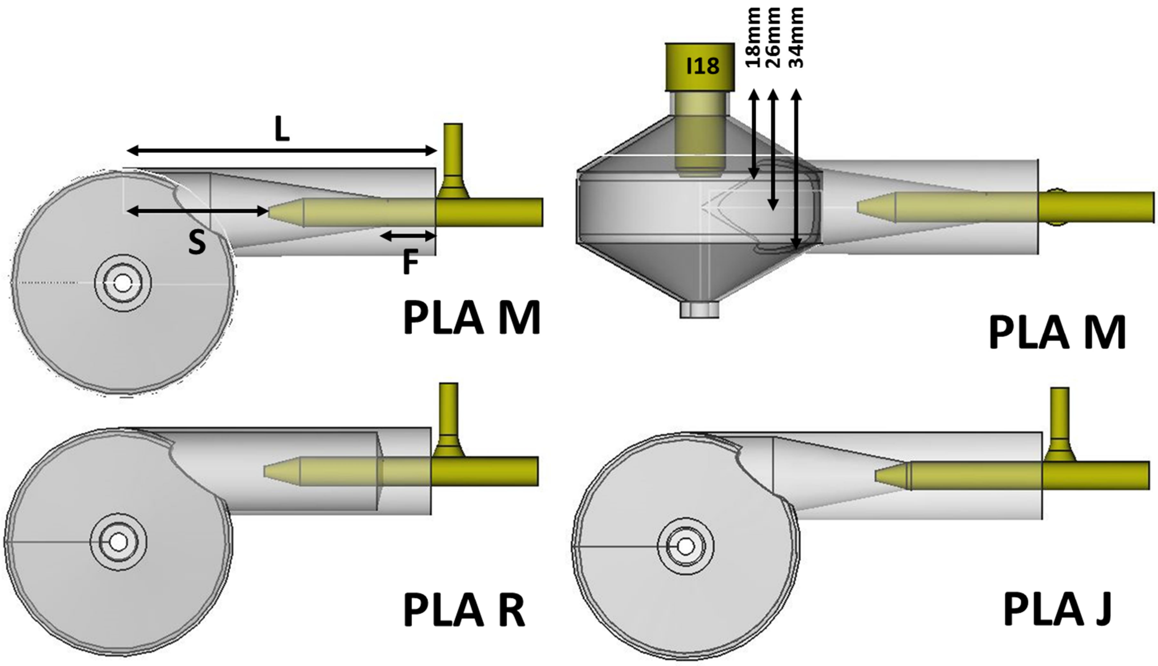

Figure 2 : Top and side views of various spray chambers with nebulizer and transfer tube I18

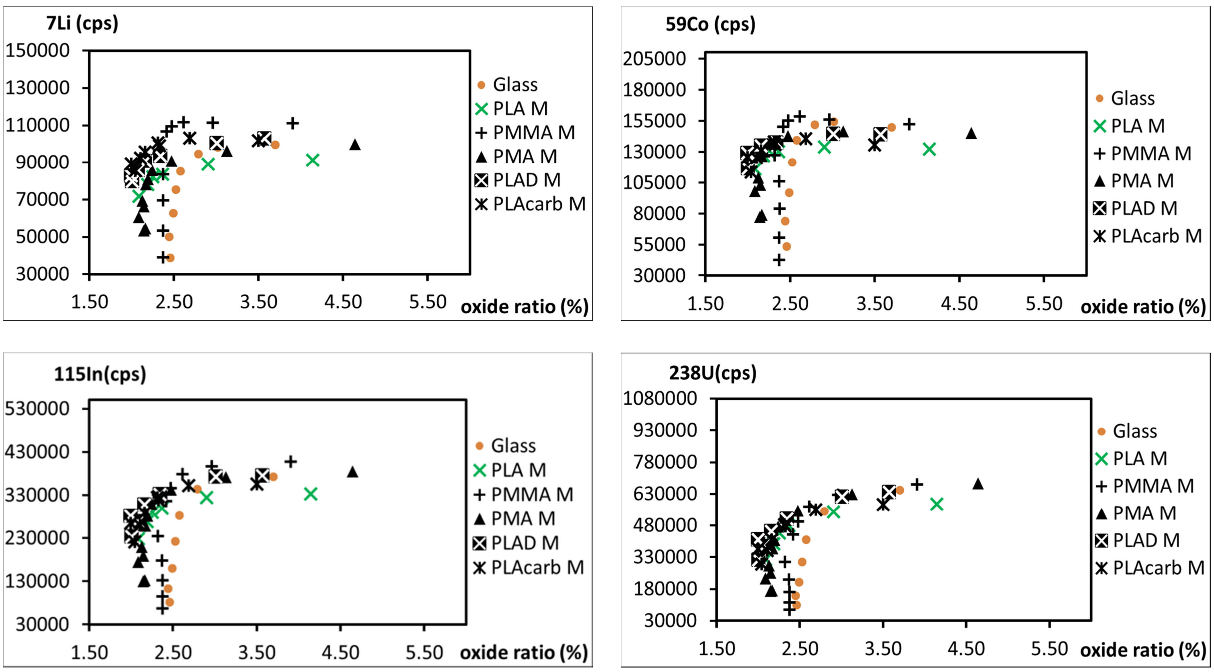

Figure 3 : Signal intensity versus cerium oxide ratios at ambient temperature for spray chambers with M geometry

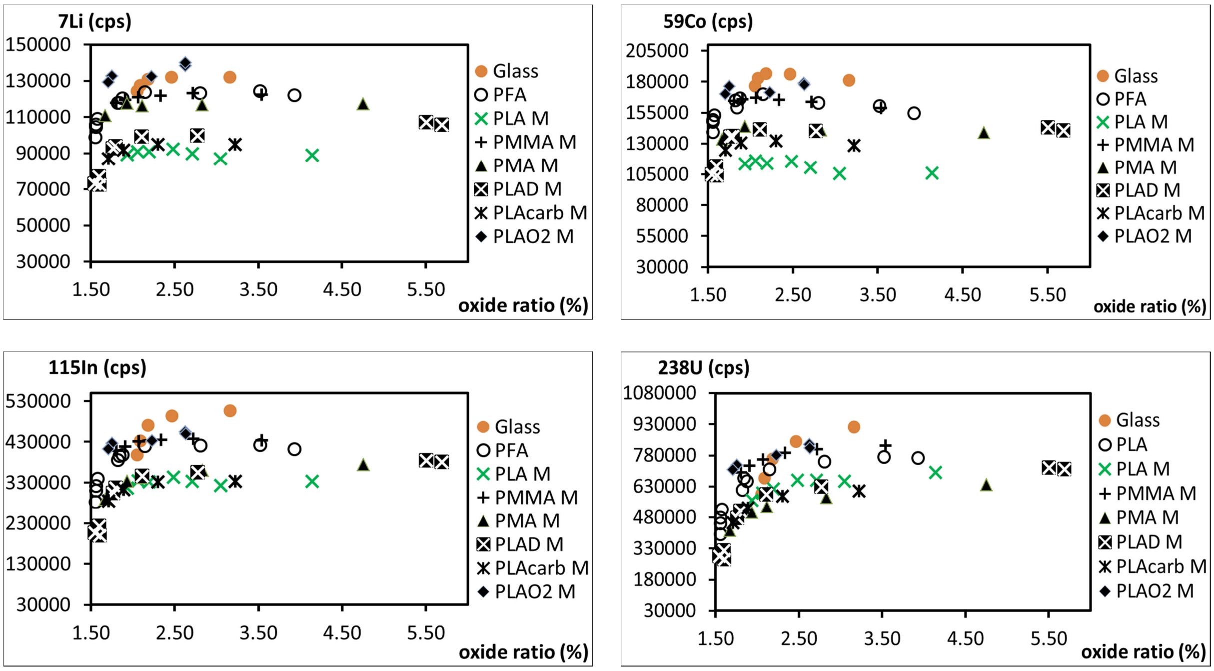

Figure 4 : Signal intensity versus cerium oxide ratios at low temperature for spray chambers with M geometry

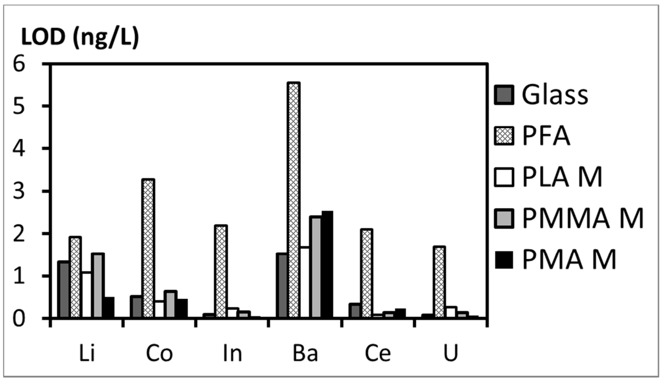

Figure 5 : LOD for several spray chambers at low temperature

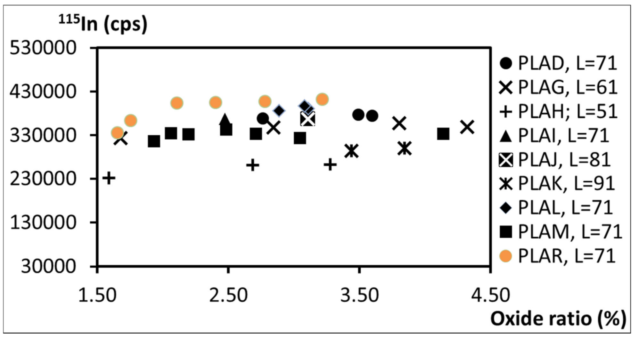

Figure 6 : 115In signal intensity versus cerium oxide ratios at low temperature for spray chambers geometries described in Table 3.

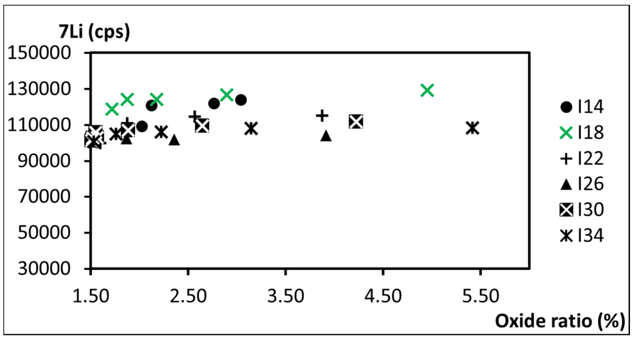

Figure 7 : Transfer tube influence on ^{7}Li signal intensity and cerium oxide ratio for PMMA M spray chamber at low temperature

References

1. AM Platform, *Additive Manufacturing; Strategic Research Agenda*, TCI. 2014.
2. M. D. Symes, P. J. Kitson, J. Yan, C. J. Richmond, G. J. T. Cooper, R. W. Bowman, T. Vilbrandt and L. Cronin, *Nature Chemistry*, 2012, **4**, 349-354. DOI: 10.1038/nchem.1313.
3. J. Todoli and J. Mermet, *Liquid Sample Introduction in ICP Spectrometry: A practical Guide*. 2008.
4. M. G. Minnich, J. A. McLean and A. Montaser, *Spectrochimica Acta Part B-Atomic Spectroscopy*, 2001, **56**, 1113-1126.
5. V. Geertsen, P. Lemaitre, M. Tabarant and F. Chartier, *Journal of Analytical Atomic Spectrometry*, 2012, **27**, 146-158. DOI: 10.1039/c1ja10255a.
6. D. S. Engstrom, B. Porter, M. Pacios and H. Bhaskaran, *Journal of Materials Research*, 2014, **29**, 1792-1816. DOI: 10.1557/jmr.2014.159.
7. N. H. Bings, J. O. O. von Niessen and J. N. Schaper, *Spectrochimica Acta Part B-Atomic Spectroscopy*, 2014, **100**, 14-37. DOI: 10.1016/j.sab.2014.08.011.
8. J. L. Todoli and J. M. Mermet, *Spectrochimica Acta Part B-Atomic Spectroscopy*, 2006, **61**, 239-283. DOI: 10.1016/j.sab.2005.12.010.
9. B. L. Sharp, N. W. Barnett, J. C. Burridge and J. F. Tyson, *Journal of Analytical Atomic Spectrometry*, 1987, **2**, R167-R210. DOI: 10.1039/ja987020167r.
10. S. Maestre, Thesis University of Alicante, 2002.
11. S. Greenfield and D. T. Burns, *Analytica Chimica Acta*, 1980, **113**, 205-220. DOI: 10.1016/s0003-2670(01)93734-1.
12. B. Thelin, *Analyst*, 1981, **106**, 54-59. DOI: 10.1039/an9810600054.
13. L. Ebdon and M. R. Cave, *Analyst*, 1982, **107**, 172-178. DOI: 10.1039/an9820700172.
14. P. A. Vieira, H. Zhizhuang, S. K. Chan and A. Montaser, *Applied Spectroscopy*, 1986, **40**, 1141-1146. DOI: 10.1366/0003702864507512.
15. P. N. Keliher, D. J. Gerth, J. L. Snyder, H. Wang and S. F. Zhu, *Analytical Chemistry*, 1988, **60**, R342-R368.
16. X. H. Zhang, H. F. Li and Y. F. Yang, *Talanta*, 1995, **42**, 1959-1963. DOI: 10.1016/0039-9140(95)01675-9.
17. L. C. Trevizan, E. C. Vieira, A. R. A. Nogueira and J. A. Nobrega, *Spectrochimica Acta Part B-Atomic Spectroscopy*, 2005, **60**, 575-581. DOI: 10.1016/j.sab.2005.02.014.
18. A. Asfaw and G. Wibetoe, *Journal of Analytical Atomic Spectrometry*, 2007, **22**, 158-163. DOI: 10.1039/b609531c.
19. M. Wu and G. M. Hieftje, *Applied Spectroscopy*, 1992, **46**, 1912-1918. DOI: 10.1366/0003702924123647.
20. M. Wu, Y. Madrid, J. A. Auxier and G. M. Hieftje, *Analytica Chimica Acta*, 1994, **286**, 155-167. DOI: 10.1016/0003-2670(94)80156-8.
21. J. L. Todoli, S. Maestre, J. Mora, A. Canals and V. Hernandis, *Fresenius Journal of Analytical Chemistry*, 2000, **368**, 773-779. DOI: 10.1007/s002160000583.
22. J. L. Todoli, J. M. Mermet, A. Canals and V. Hernandis, *Journal of Analytical Atomic Spectrometry*, 1998, **13**, 55-62. DOI: 10.1039/a704342b.
23. G. Schaldach, H. Berndt and B. L. Sharp, *Journal of Analytical Atomic Spectrometry*, 2003, **18**, 742-750. DOI: 10.1039/b302052e.
24. D. F. Thompson, *Journal of Analytical Atomic Spectrometry*, 2014.
25. G. Schaldach, L. Berger, I. Razilov and H. Berndt, *Journal of Analytical Atomic Spectrometry*, 2002, **17**, 334-344. DOI: 10.1039/b106024b.
26. A. Frohn and N. Roth, *Dynamics of drplets*, Springler Berlin. 2000.
27. Y. Makonnen, J. Burgener and D. Beauchemin, *Journal of Analytical Atomic Spectrometry*, 2015, **30**, 214-224. DOI: 10.1039/c4ja00258j.
28. Y. Zhao, A. Fina, A. Venturello and F. Geobaldo, *Applied Surface Science*, 2013, **283**, 181-187. DOI: 10.1016/j.apsusc.2013.06.078.
29. R. M. Rasal, A. V. Janorkar and D. E. Hirt, *Progress in Polymer Science*, 2010, **35**, 338-356. DOI: 10.1016/j.progpolymsci.2009.12.003.

30. L. Chaozong, N. Cui, N. M. D. Brown and B. J. Meenan, *Surface & Coatings Technology*, 2004, **185**, 311-320. DOI: 10.1016/j.surfcoat.2004.01.024.
31. J. L. Todoli and V. Hernandis, *Journal of Analytical Atomic Spectrometry*, 1999, **14**, 1289-1295.
32. B. L. Sharp, *Journal of Analytical Atomic Spectrometry*, 1988, **3**, 939-963. DOI: 10.1039/ja9880300939.
33. B. L. Sharp, *Journal of Analytical Atomic Spectrometry*, 1988, **3**, 613-652.